Hindawi
Journal of Control Science and Engineering
Volume 2020, Article ID 2045634, 11 pages
https://doi.org/10.1155/2020/2045634

Research Article

Research on Key Control Technology of Intelligent Rolling Contact Fatigue Test Facility

Jianyao Li,[1] Juke Liang,[2] Gubo Chen,[1] and Yan Yang[1]

[1]*Chongqing University of Technology, Chongqing 400054, China*
[2]*Chongqing Haohan Co. Ltd., Chongqing 400050, China*

Correspondence should be addressed to Yan Yang; yangyan@cqut.edu.cn

Received 6 November 2019; Revised 1 February 2020; Accepted 10 February 2020; Published 16 March 2020

Academic Editor: Radek Matušů

An intelligent rolling contact fatigue test equipment is developed, and the control methods are presented. For obtaining the slip accurately, the control method based on master-slave synchronization is proposed. For controlling the loads in high precision, the control method took into consideration the influence by two factors, displacement and the load. The nonlinear interference and excess torque in load control are effectively suppressed. Based on the SIMOTION D425 which is the Siemens integrated motion control system, the control system architecture of the intelligent rolling contact fatigue test equipment is constructed. The solutions of slip ratio and the experimental load controlled by these methods are satisfactory with the requirement of design precision. In the validation experiment, the load control accuracy is ±3%, the average error of load control is 1.77%, and the average error of slip control is 0.26%. The experiment results show the proposed control methods are feasible and effective.

1. Introduction

The rolling contact fatigue test is the main method to study the rolling contact fatigue performance of materials under simulated working conditions. Rolling contact fatigue test machine is the major equipment for the rolling contact fatigue test, which is used to test the contact fatigue life of gears, bearings, and other basic part materials [1]. In order to ensure that the fatigue test can obtain accurate and reliable test results, the testing machine needs to simulate the test conditions accurately and has the function of running continuously for a long time and recording the operation data accurately. Therefore, a stable and reliable system is an important guarantee for the normal operation of the testing machine.

In recent years, related research on fatigue testing technology has attracted more and more attention from scholars around the world [2–6]. Hua et al. developed a special test device to test and evaluate the fatigue of artificial hip joint effectively [7]; Tan et al. designed energy-saving transmission fatigue tester system using common DC bus energy recovery technology that can adapt to high-power, high-speed test environment, and energy-saving effect up to 90% [8]; Bai et al. proposed a new method of resonant fatigue test using 2D high-frequency rotary valve control hydraulic cylinder, which can improve the frequency of electrohydraulic fatigue test effectively [9]; Li et al. introduced a new type of testing machine that can perform rolling fatigue test on the bearing ball under large loads and high speed, and the test system monitors various signals at the same time, which can analyze and determine the fatigue status [10]; and Schneider et al. developed a large-scale beam resonant contact fatigue testing machine. The resonance test system is adopted, so it has higher load frequency and reduces the test time and cost greatly [11].

In addition, the testing machine measurement and control system also has done a lot of research; Manoj et al. developed a three-rig rolling contact fatigue testing machine, which adopts the AXPERT VT300 controller to achieve accurate control of test speed [12]; and Yang et al. developed a lever-loaded rolling contact fatigue testing machine for superhard coated materials. The control system adopts a combination of computer and speed controller to achieve accurate monitoring and diagnosis of fatigue state [13].

Wang et al. developed a five-ball fatigue testing machine with pneumatic loading, which uses an intelligent electronic control system with tracking filter to realize the functions of large load and high-speed running [14]; You developed a double-lower position machine control system based on EDC220 controller and s7-300 PLC for the electrohydraulic servo fatigue testing machine, which solved measurement missing problem during a long run effectively [15]; Tao et al. developed the alloy material fatigue test control mechanism system based on STM32 single chip microcomputer and realized the functions of stepless speed regulation, interval control, and fatigue frequency statistics of the testing machine [16].

Although the existing control system of fatigue testing machine can basically meet the test requirements, some test conditions cannot be accurately controlled such as slip rate and test load. Manual shutdown is required to detect fatigue state. The judgment of the fatigue state is not accurate, and the initial fatigue state cannot be captured. The online detection ability is not strong, and the real-time and accurate detection of each test parameter cannot be made depending on a single detecting signal. For solving above problems, self-designed intelligent rolling contact fatigue testing machine uses machine vision and vibration analysis for real-time detection of the fatigue state. The compound closed-loop control is adopted to accurately simulate the test conditions. The developed software system can record the data and automatically operate to achieve the goal of unmanned safeguarding.

In this paper, the test slip rate and load control system are designed with SIMOTION D425 controller as the core, and the accurate simulation of rolling contact fatigue test condition of sliding friction pair is realized. The human-machine interaction system of rolling contact fatigue test was developed based on LabVIEW architecture, and real-time acquisition of instruction input and feedback data was realized. The feasibility and rationality of the control method of test slip rate and test load were verified through the test, and the control accuracy was analyzed through the test data.

2. Principle and Requirement of Fatigue Test

2.1. Fatigue Test Principle. Rolling contact fatigue refers to the surface fatigue failure phenomenon caused by long-term repeated contact pressure stress on certain surfaces during pure rolling or rolling sliding friction. The contact forms are mainly divided into point contact and line contact. The relevant research in this paper primarily focuses on the linear contact rolling contact fatigue test. The test principle is shown in Figure 1.

In Figure 1, the test roller and mating roller are assembled on the corresponding spindle, and the power transmitted to each spindle drives their rotation. By adjusting the speed of the two spindles, different slip rates can be simulated. The contact compressive stress between the test roller and the mating roller is indirectly provided by the load applied to the test module spindle.

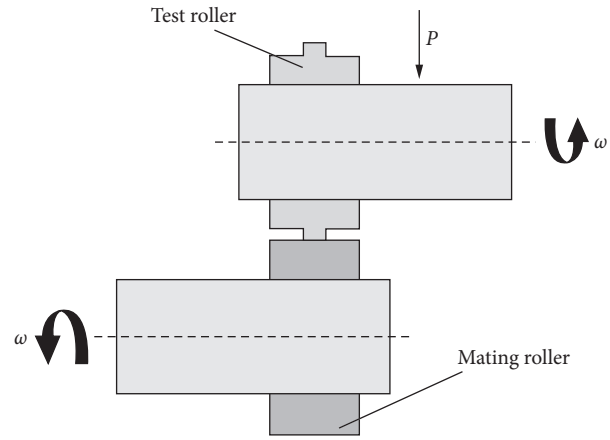

Figure 1: Principle of linear contact rolling contact fatigue test.

2.2. Requirements of Fatigue Test Control. To ensure the accuracy of the rolling contact fatigue test, it is required to simulate the real rolling contact conditions of materials or parts as much as possible. Combined with the requirements of the existing industry standards, the rolling contact fatigue testing machine shall meet the following two requirements:

(a) The relative motion state of the two samples remains unchanged that the slip rate of the test remains unchanged

(b) The fluctuation of contact compressive stress of two samples should be as small as possible; that is, the error of test load should be as small as possible

3. Mechanical Structure

3.1. Main Structure of the Test Machine. Based on the modular design method, the structure of rolling contact fatigue testing machine is divided into test module, accompany module, and loading module. The main functions of each module are as follows:

(a) Test module: the test roller is assembled at the spindle end of the module according to the accuracy requirements of relevant standards, and the test roller is driven by the servo motor of the module to rotate to simulate the working conditions of the test system.

(b) Accompany module: according to the accuracy requirements, mating roller is assembled at the spindle end of the module and drives the servo motor of the module to the mating roller to rotate to simulate the working condition of the accompany system.

(c) Loading module: it provides contact compressive stress for test roller and mating roller. The load is controlled by the servo cylinder.

The structure and composition of the testing machine are shown in Figure 2, and the main control indexes and accuracy are shown in Table 1.

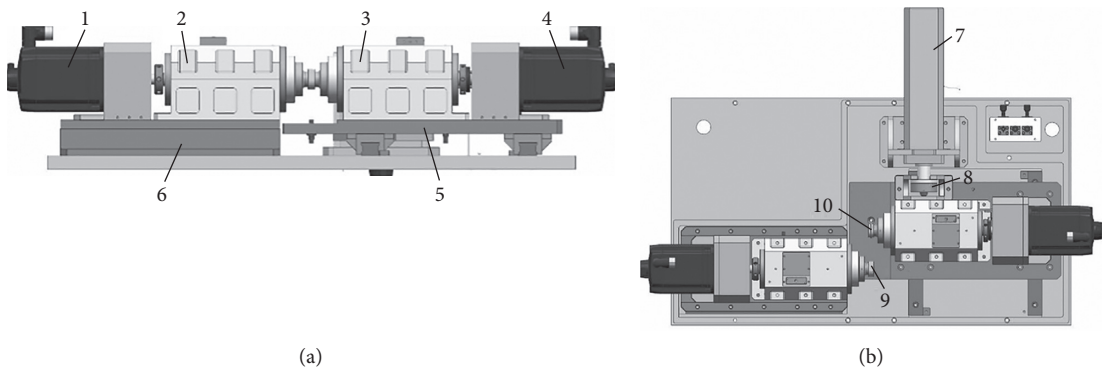

Figure 2: Structure composition of testing machine: (a) main view; (b) top view. 1, accompany module drive motor; 2, accompany module headstock; 3, test module headstock; 4, test module drive motor; 5, test module; 6, accompany module; 7, loading module; 8, load sensor; 9, mating roller; 10, test roller.

Table 1: Main control index and precision requirement.

No.	Name	Parameter
1	Slip rate	1%–20%
2	Loading range	0–2000 kg
3	Slip control accuracy	±1%
4	Test load dynamic accuracy	±3%

3.2. Visual Detection Structure. At present, in the rolling contact fatigue test, contact fatigue state is often detected by acoustic emission, vibration signal, ultrasonic wave, and other detection methods. Although these methods can detect sample fatigue, they cannot visually record the evolution of rolling contact fatigue, let alone quantify fatigue damage [17].

The machine adopts a machine vision detection method, which can not only detect the fatigue state in real time but also analyze the fatigue performance data online quantitatively. The structure of fatigue state visual detection is shown in Figure 3. The CCD camera and the light source are placed on the truss of the gantry fixed on the testbed, which can not only conveniently adjust the position of the camera but also reduce the influence of the vibration of the test machine on the camera compared with the general single-arm structure. The test roller is placed in an oil box with a small hole at the top, and visual images can be acquired while the oil is lubricated.

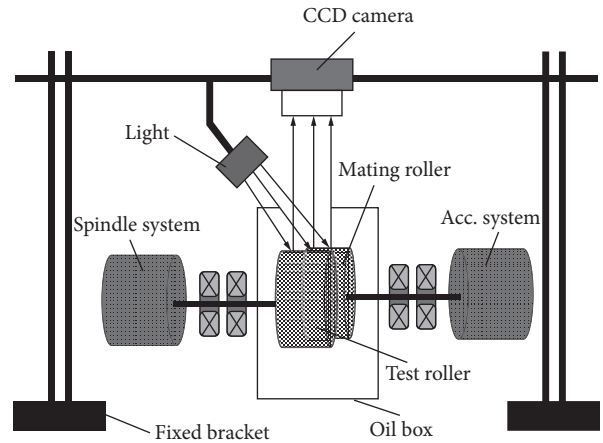

Figure 3: Structure diagram of fatigue vision detection.

4. The Proposed Method

4.1. Slip Rate Control Scheme. According to the requirements of the experiment, the slip rate between the test roller and the mating roller is selected based on the actual working condition of the sample material. For example, simulating rolling bearing materials generally select 5% and gear materials generally 10~20%. The slip rate is generally regulated by instruction allocation. In this way, the calculated two spindle speeds are taken as the benchmark, and the speed of each motor is separately controlled to achieve the purpose of regulating the slip rate. When the speed of the two axis fluctuates due to the interference of external factors, the slip error will be increase exponentially.

To reduce the control error of slip rate, the control strategy of master-slave synchronization is introduced. The method takes the command speed of the test master as the master value and apply it as the input of the speed of the slave axis (that is, the auxiliary test spindle) after synchronous operation to realize the linear transfer of the speed of the master and slave. It avoids the superposition of errors in individual control. Specifically, the electronic gear of SIMOTION D425 controller is adopted to complete the system calculation and realize the master-slave synchronization control within the servo clock cycle of 24 ms. The principle is shown in Figure 4.

Combined with industry standards and master-slave synchronous movement control requirements of testing machine, the governing equations of spindle speed, test spindle speed, and slip rate are shown in equation (1) under the condition that the test spindle speed and slip rate are set by instruction distribution:

$$v_{\text{acc}} = \frac{v_{\text{main}}}{1-h}, \tag{1}$$

where v_{acc} is the accompany test spindle speed, v_{main} is the test spindle speed, and h is the slip rate.

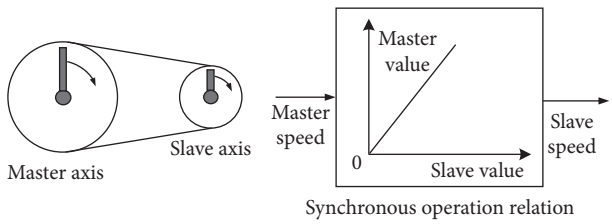

Figure 4: Electronic gear synchronization.

4.2. Load Control Scheme. Servo electric cylinder is adopted in this paper to realize the electric loading function, and its hardware system composition is shown in Figure 5. According to the instruction of the host computer, the controller drives the servo cylinder to apply load to the test system. The load signal measured by the pressure sensor is fed back to the controller for feedback control after signal conditioning, to attain the force closed-loop control function of the load.

The electric loading system is a typical passive loading system. The active movement of the loaded part brings about position change and causes redundant torque. The excess torque affects the control accuracy of the loading system, and reducing the excess torque is the key problem of the electric loading system [18, 19]. During the loading process of the fatigue testing machine, the position interference of the high-speed spindle system will cause redundant torque, which will affect the accuracy of the servo cylinder loading seriously.

To meet the stability of the dynamic loading of the testing machine, the force closed-loop control method using a pressure sensor as the load measuring element is usually adopted. Figure 6 is the structure block diagram and corresponding mathematical model of force closed-loop stability control.

In Figure 6, F_R^* and F_T are the expected loading force and the actual output loading force of the system. $G_F(s)$ and $G(s)$ are the transfer function of force stability controller, speed closed-loop controller of driver, and servo cylinder. K_S is the strain constant of the pressure sensor, and $r(s)$ is the time-varying interference signal caused by active movement of the spindle system. The transfer function F_T under the output Laplace transform of the double closed-loop control system is

$$F_T = \frac{G_F(s)G(s)K_S F_R^* + r(s)}{1 + K_S G_F(s)G(s)}. \tag{2}$$

In the design process of the correction ring, it can meet the following requirements within the required frequency band:

$$\left|K_S G_F(s)G(s)\right| \gg 1. \tag{3}$$

Then, equation (3) can be approximately simplified to

$$F_T = F_R^* + \frac{r(s)}{K_S G_F(s)G(s)}. \tag{4}$$

It can be seen from equation (4) that, in the single-loop control, the suppression of interference $r(s)$ is completed by the correction loop. However, only $G_F(s)$ is used to suppress interference, and its regulating ability is often limited. At the same time, the change in system characteristics will also affect the stability of the system. Therefore, this method is difficult to achieve higher system dynamic performance.

To further realize the stability of dynamic loading performance, this paper proposes a position-load composite control method of position closed-loop compensation and string speed closed-loop control, whose structure block diagram and mathematical model are shown in Figure 7.

In Figure 7, θ_R^* and θ are the reference position and the actual position of the servo cylinder. $G_\omega(s)$ and $G_\theta(s)$ are the transfer function of the velocity closed-loop controller and position closed-loop controller.

The transfer function formula (5) under the position-load composite control is obtained from the mathematical model of Figure 7(b):

$$F_T = \frac{G_F(s)G_\omega(s)G(s)K_S F_R^* + G_\theta(s)G_\omega(s)G(s)\theta_R^*}{1 + G_F(s)G_\omega(s)G(s)K_S + G_\omega(s)G(s)s + G_\theta(s)G_\omega(s)G(s)} - \frac{K_S\left[1 + G_\omega(s)G(s)s + G_\theta(s)G_\omega(s)G(s)\right]\theta + r(s)}{1 + G_F(s)G_\omega(s)G(s)K_S + G_\omega(s)G(s)s + G_\theta(s)G_\omega(s)G(s)}. \tag{5}$$

In the design process of the correction ring, it can meet the following requirements within the required frequency band:

$$\left|G_\omega(s)G(s)\left(K_S G_F(s) + G_\theta(s) + s\right)\right| \gg 1. \tag{6}$$

Equation (5) can be approximately simplified to equation (7):

$$F_T = \frac{G_F(s)K_S F_R^*}{K_S G_F(s) + G_\theta(s) + s} + \frac{K_S G_\theta(s)\theta_R^*}{K_S G_F(s) + G_\theta(s) + s} - \frac{K_S G_\theta(s)\theta}{K_S G_F(s) + G_\theta(s) + s} - \frac{K_S \theta s}{K_S G_F(s) + G_\theta(s) + s} + \frac{r(s)}{G_\omega(s)\left(K_S G_F(s)G(s) + G_\theta(s)G(s) + sG(s)\right)}. \tag{7}$$

It can be seen from equation (7) that, in the position-load composite control, the suppression of interference signal $r(s)$ mainly realized through $G_\omega(s)$, $G_\theta(s)$, and $G_F(s)$ also plays an auxiliary regulating role, which has obvious performance improvement compared with the single closed-loop control system.

For the system with output y under the action of input u and interference r, its anti-interference ability can be measured by the signal-to-noise ratio $A = (y/u)/(y/r)$. The larger the value is, the stronger its anti-interference ability will be. The signal-to-noise ratio of the controllable closed-loop control system and the composite control system is

$$A_1 = \frac{F_T/F_R^*}{F_T/r} = G_F(s)G(s), \tag{8}$$

$$A_2 = \frac{F_T/F_R^*}{F_T/r} = G_F(s)G_\omega(s)G(s). \tag{9}$$

In the composite control, the velocity loop is in the lower order of the inner loop, and its gain coefficient can be larger.

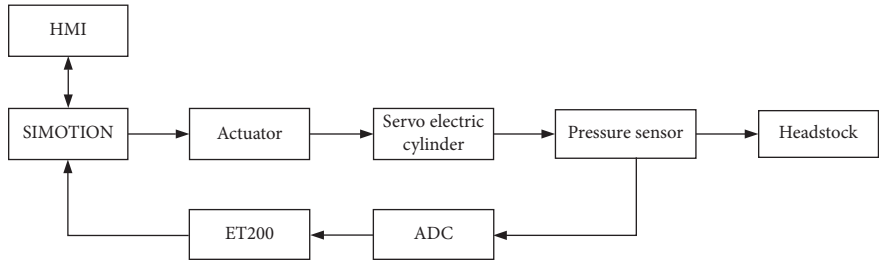

Figure 5: Test machine loading hardware system composition.

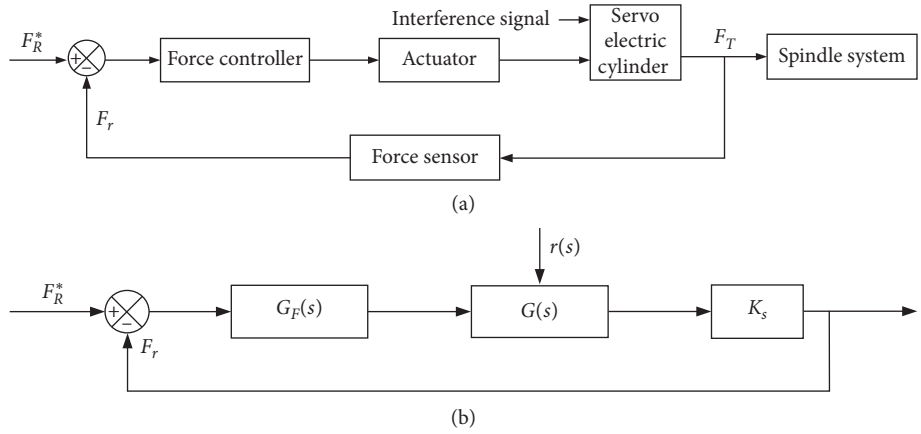

Figure 6: Force closed-loop control model: (a) force closed-loop control structure; (b) corresponding mathematical model.

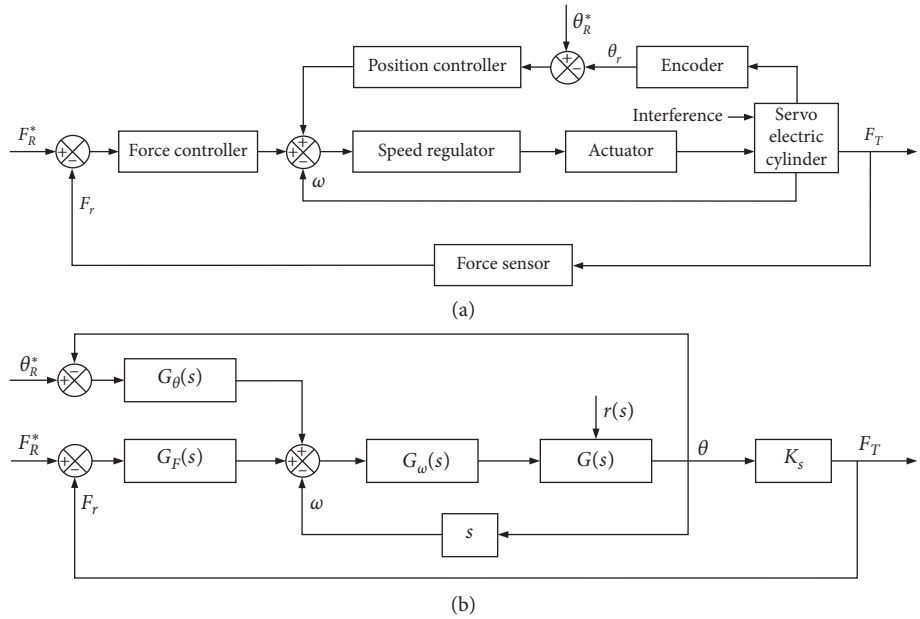

Figure 7: Composite closed-loop control model: (a) composite closed-loop control block; (b) corresponding mathematical model.

According to equations (8) and (9), we can obtain $|A_1| > |A_2|$, so the composite control system has a stronger ability to overcome interference than force closed-loop control. At the same time, the position closed loop in the composite control system can also act on the speed regulation quickly, which improves the loop gain and phase margin of the system and improves the dynamic performance of the system.

4.3. Load Control Simulation Analysis. The electric servo loading system is composed of synchronous servo motor, motor controller, and the ball screw reducer. The rotating motion of the motor is changed to linear motion by ball screw for resistance loading. When loaded, the motor armature winding voltage balance equation, electromagnetic torque equation, and the motor shaft torque balance equation are as follows:

$$\begin{cases} K_v U_q = L\dfrac{\mathrm{d}i_q}{\mathrm{d}t} + Ri_q + C_r\omega, \\ T_m = K_m K_p i_q, \\ J\dfrac{\mathrm{d}\omega}{\mathrm{d}t} = T_m - T_i - B\omega. \end{cases} \tag{10}$$

According to the Laplace transform in equation (10), the control voltage U_q is taken as the input. The displacement θ of the electric cylinder is the output, and the transfer function of the servo loading system can be obtained as follows:

$$G(s) = \frac{K_v K_p K_m}{s\left[\left(Ls + R + K_p\right)(Js + B) + K_m C_r\right]}, \tag{11}$$

where L is the motor armature inductance, R is the armature resistance, J is equivalent to the moment of inertia on the shaft of the motor, B is the damping coefficient, K_v is the current conversion coefficient of control voltage U_q, K_p is the current control gain, K_m is the motor torque coefficient, and C_r is the back EMF coefficient. The structure diagram of the servo loading system is shown in Figure 8.

The external loop of the loading system adopts the PID force closed-loop control strategy to suppress the friction damping of the cylinder, external disturbance, and other nonlinear factors. It improves the following ability and loading accuracy of the system. The internal velocity closed-loop and position loop compensation are designed as an active PI regulator realized by the integrated operational amplifier, which can compensate the force closed loop, improve the stiffness of the system, suppress the internal disturbance quickly, and reduce the influence of load parameters.

The simulation system was built in Simulink. When the input was set as constant load 5 kN, the simulation comparison result of the control effect of the force closed-loop and the compound closed-loop under random interference is shown in Figure 9. As can be seen from the figure, the response speed of the two is quite similar, but the anti-interference capability of the compound control is stronger, and the fluctuation error is reduced from 2.7% to 0.8%.

5. Control System of Testing Machine

5.1. Hardware System. The integrated motion control system with both logic control and process control functions can quickly and reliably control multiple servo motors [20, 21]. In this paper, SIMOTION is adopted as the controller of the integrated motion control system. It controls the speed control of the driving motor of the two axis and the force position of the loading motor. The system composition is shown in Figure 10.

In Figure 10, the functions of each hardware module are detailed as follows:

(a) SITOP module: it provides stable and reliable 24 V DC power for control system.

(b) Electric reactor: it limits the sudden change of AC grid voltage and smooth peak voltage to ensure the stability of system power supply.

(c) SIMOTION D425: the control core of the testing machine is used for the logic control, process control, motion control, data processing, and communication.

(d) PC: it sends operation instruction to SIMOTION through communication protocol. After receiving the instruction, SIMOTION carries out logical calculation and generates control pulse and then transmits it to motor module for servo control through DRIVE-CLIQ interface.

(e) Distributed I/O ET200 and 13 bit ADC: data acquisition module can be combined to collect 8-channel signals at the same time. It can collect different types of test data quickly and accurately.

(f) Active regulating power module ALM: it has the functions of rectification and energy feedback and can also adjust the phase angle of DC bus voltage and AC side voltage and current, to ensure the reliability and efficiency of the motor.

(g) Single-shaft motor DRIVE module: it accepts the control parameters through the DRIVE-CLIQ interface and drives the servo motor through the DC bus to realize the servo control.

After the hardware system is built, the hardware configuration of the system is also required. SIMOTION hardware configuration mainly includes hardware configuration, SINAMICS configuration, and shaft process configuration [22].

Hardware configuration is based on the feature and number of input and output signals of each module. According to the hardware composition, the hardware configuration of the testing machine is shown in Figure 11.

SINAMICS driver configuration uses software to automatically identify the device and configuration with DRIVE-CLIQ interface. The driving system is configured to run and test whether the rotation direction and encoder direction of the motor are consistent with the design. At the same time, the static identification of the motor model parameters and the automatic optimization of the controller parameters are carried out.

The shaft is an abstraction of the servo driver and encoder called the process object. The control system can realize the functions of enabling activation, absolute motion,

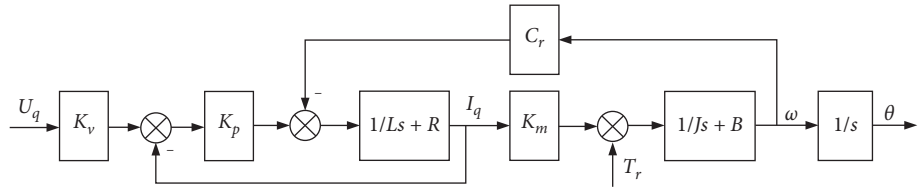

Figure 8: Load system structure diagram.

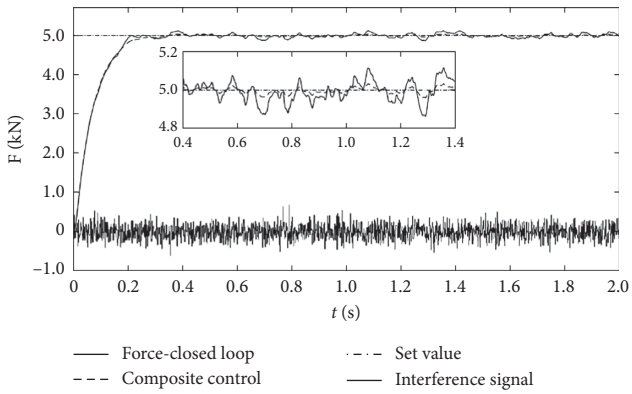

Figure 9: Force closed-loop and composite control anti-interference simulation contrast curve.

relative motion, and state monitoring through control instructions and variables. In the process of creating shaft process, objects need to specify the name of the shaft, types, process, and connection driver. Machine configuration of the three-axis process is shown in Table 2.

5.2. Software System. The software of the control system is mainly to complete the shaft of the motor motion control, logic control, data acquisition, processing, fault handling, human-computer interaction, and other functions. In this paper, the develop software SCOUT of SIMOTION controller and virtual instrument LabVIEW are used as the software development platform, and the driver software and human-machine interaction software of the lower position machine of the testing machine are designed with a modular structure.

The main control program of the test machine was developed under the SCOUT environment, mainly using MCC and LAD programming methods to realize the functions of motion control, logic control, and fault handling. The HMI is mainly used to set the running parameters of the testing machine, display real-time data, and detect and store data. Host computer based on LabVIEW and SIMATIC NET platform can easily access the underlying program variables through the OPC server on the PC and realizes the reliable reading and writing of data.

6. Experiments

6.1. Establishment of Experimental Environment. The motion control system of the testing machine designed in this paper is mounted on an independently developed rolling contact fatigue testing machine, and the hardware environment for the functional test of the motion control system is built. The test site environment is shown in Figure 12.

6.2. Experimental Scheme Design

6.2.1. Slip Control Verification Scheme. To verify the function and accuracy of slip control, the test scheme of slip control function and accuracy verification shown in Table 3 is designed under the condition of consistent test conditions such as test load.

6.2.2. Load Control Verification Scheme. To verify the function and accuracy of test load control, the test load control function and accuracy verification test scheme as shown in Table 4 are designed under the condition that test conditions such as slip rate are consistent.

6.3. Experimental Results and Analysis

6.3.1. Slip Rate Control Test Results and Analysis. According to slip rate control function and accuracy verification test scheme, the spindle speed and slip rate set value of the sample are input into the test machine through the human-computer interaction software. Under the condition that the test load is the same, the rotation speed data of 120 continuous test spindles are randomly collected for 9 test conditions to verify the control function of slip rate and analyze the control accuracy after the equipment is up and running stably. The statistical analysis results are shown in Figures 13–15.

Combined with experimental data and Figure 13, the following is obtained:

(a) The average slip rate of test 1 is 5.043%, and the slip rate control error is 0.86%

(b) The average slip rate of test 4 is 4.997%, and the slip rate control error is 0.06%

(c) The average slip rate of test 7 is 4.991%, and the slip rate control error is 0.18%

Combined with experimental data and Figure 14, the following is obtained:

(a) The average slip rate of test 2 is 0.078%, and the slip rate control error is 0.78%

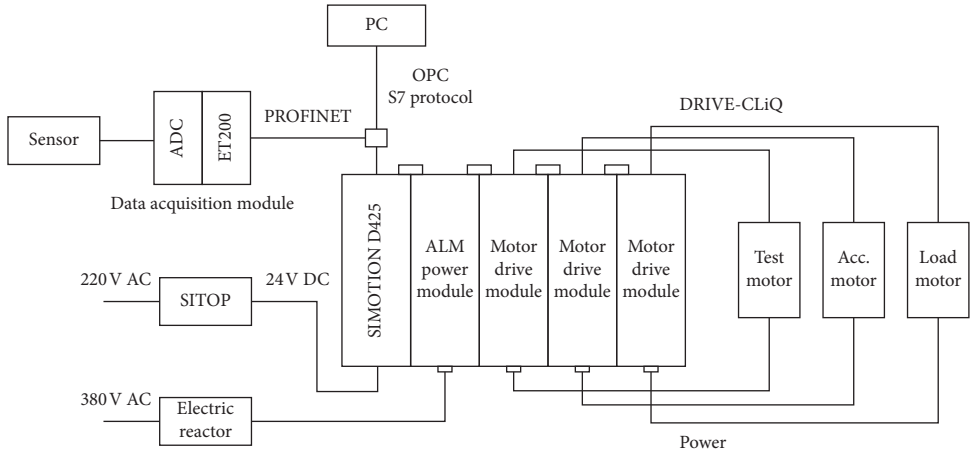

Figure 10: Testing machine hardware system composition block.

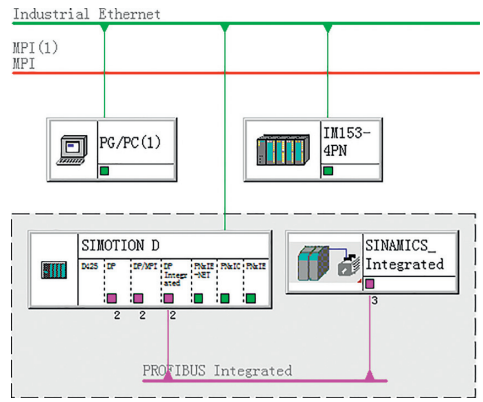

Figure 11: Testing machine hardware configuration.

Table 2: Machine working shaft process object configuration.

Name	Axis type	Axis process	Connected motor
Main axis	Electrical, rotation	Velocity	Spindle
Accom. axis	Electrical, rotation	Following	Accompany
Load axis	Electrical, straight	Position	Load

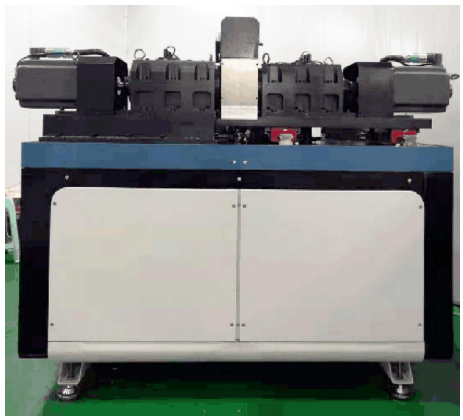

Figure 12: Experimental site environment.

Table 3: Slip control verification test scheme.

No.	Spindle speed of the test roller (r/min)	Slip rate set value (%)
Test 1	800	5
Test 2	800	10
Test 3	800	15
Test 4	1500	5
Test 5	1500	10
Test 6	1500	15
Test 7	2100	5
Test 8	2100	10
Test 9	2100	15

Table 4: Test load control verification test scheme.

No.	Test load setting (kg)
Test 1	600
Test 2	850
Test 3	1150

(b) The average slip rate of test 5 is 9.99%, and the slip rate control error is 0.01%

(c) The average slip rate of test 8 is 10.0%, and the slip rate control error is 0

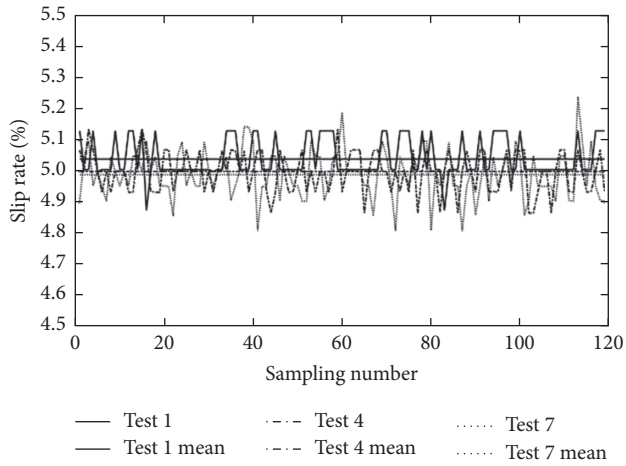

Figure 13: Tests 1, 4, and 7 slip rate statistics and mean curve.

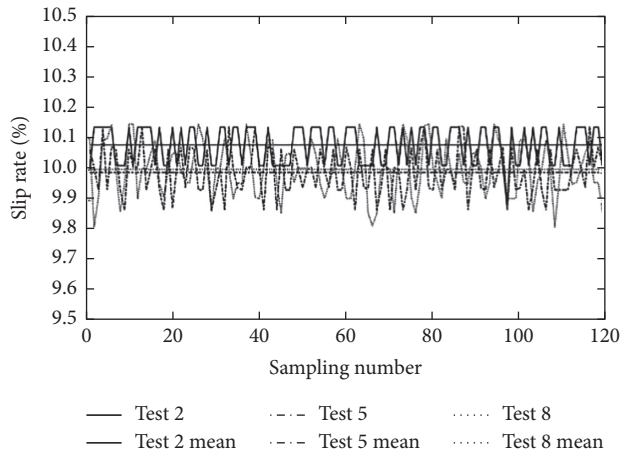

Figure 14: Tests 2, 5, and 8 slip rate statistics and mean curve.

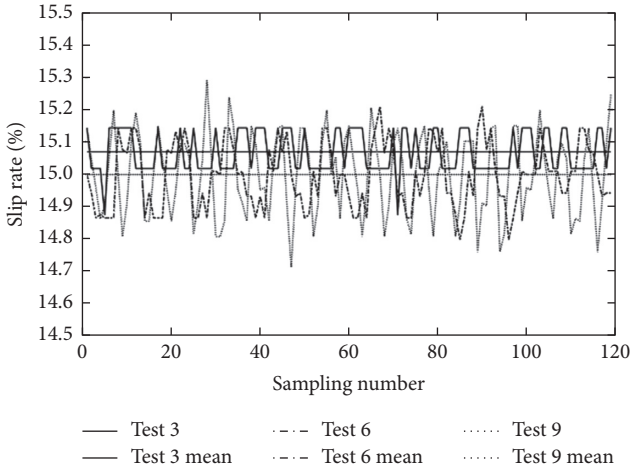

Figure 15: Tests 3, 6, and 9 slip rate statistics and mean curve.

Combined with experimental data and Figure 15, the following is obtained:

(a) The average slip rate of test 3 is 15.066%, and the slip rate control error is 0.44%

(b) The average slip rate of test 6 is 14.998%, and the slip rate control error is 0.01%

(c) The average slip rate of test 9 is 14.998%, and the slip rate control error is 0.01%

The statistical results of slip control accuracy are shown in Table 5.

Table 5 shows that the design of the motion control system can achieve the function of slip rate control, the control error is 0.26%, and control precision meets the design requirements of plus or minus 1%.

6.3.2. Load Control Test Results and Analysis. According to the load control verification test scheme, the set value of the test load was input into the human-computer interaction software. After the equipment started up and ran stably, the load data were collected at an interval of 20 min under the condition that the slip rate of the test was consistent. The 25 data points were collected under test conditions 1, 2, and 3 to analyze the accuracy of load control.

As can be seen from Figures 16(a)–16(c),

(a) The mean load of test 1 was 617.0 kg, with an average error of 2.8%

(b) The mean load of test 2 was 867.92 kg, with an average error of 2.1%

(c) The mean load of test 3 was 1154.3 kg, with an average error of 0.37%

The average error of load control in tests 1, 2, and 3 is 1.77%, which meets the design requirements of ±3%.

Table 5: Slip control accuracy statistics.

No.	Slip control accuracy (%)
Test 1	0.86
Test 2	0.78
Test 3	0.44
Test 4	0.06
Test 5	0.01
Test 6	0.01
Test 7	0.18
Test 8	0
Test 9	0.01

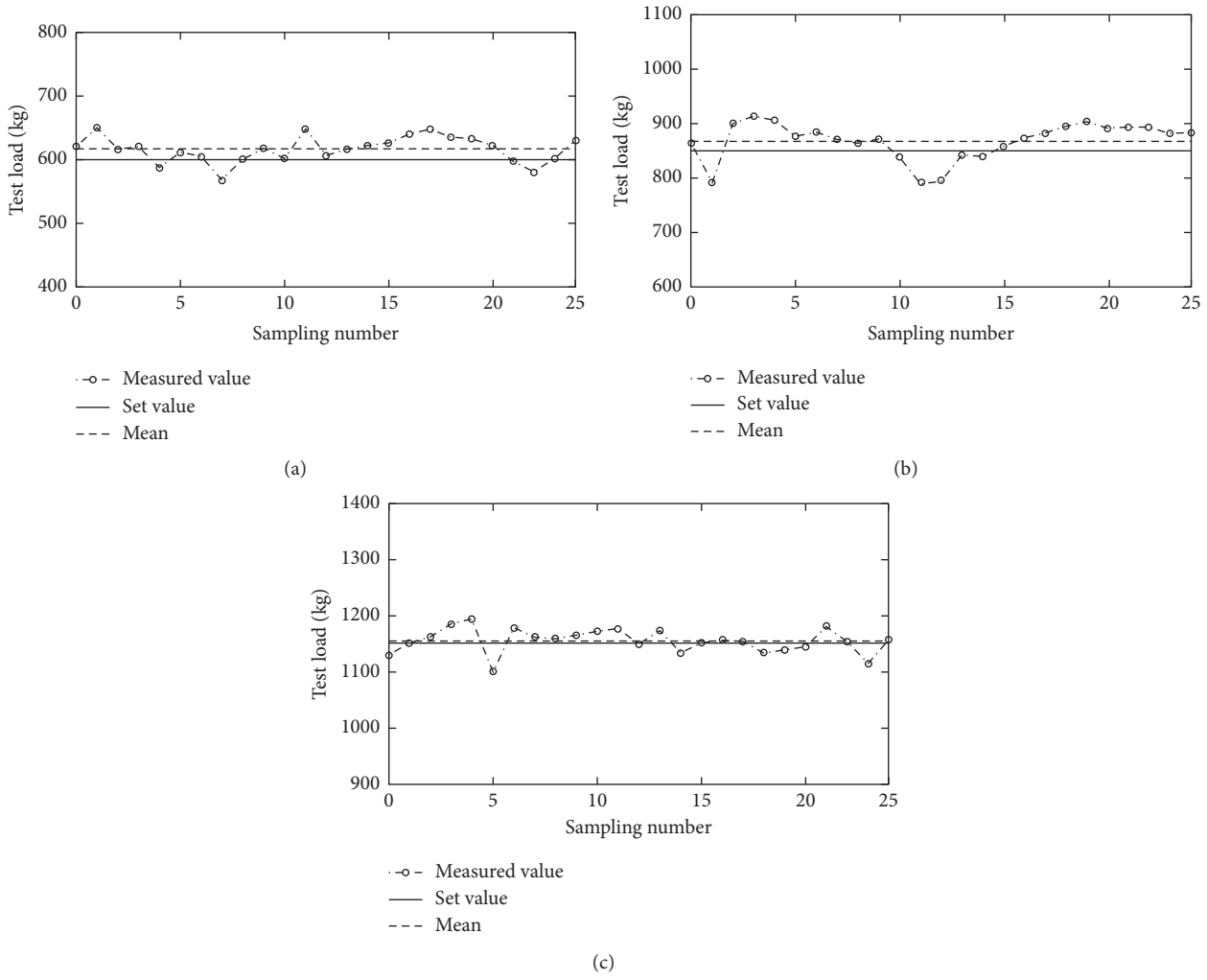

Figure 16: Test load measurement and mean curve: (a) test 1; (b) test 2; (c) test 3.

7. Conclusions

To satisfy the requirements of the rolling contact fatigue test for accurate test conditions and real-time monitoring of fatigue state, a set of testing machine motion control system based on SIMOTION D425 is proposed. The system realizes the functions of accurate control of slip ratio, test load, and real-time monitoring of fatigue data. Experimental results show that the slip rate could be regulated and controlled in the scope of design according to the test requirements, and control precision can satisfy the demands of plus or minus 1% movement control; test load could be regulated and controlled in the scope of design, and test load control in the process of precision meets the requirements of plus or minus 3% of the motion control. The control method and principle proposed in this paper are feasible and effective, which can provide a theoretical basis for the development and test of similar test equipment.

Data Availability

Readers can send e-mail to nuc2015@163.com for the test data.

Conflicts of Interest

The authors declare that they have no conflicts of interest.

References

[1] J. Wang, G. Li, H. Wang, and B. Xu, "Research status on rolling contact fatigue testing machine," *Engineering and Test*, vol. 51, pp. 1–5, 2011.

[2] J. Yu, S. Zheng, J. Feng, and T. Chen, "Research on accelerated testing method for the service-simulation fatigue test of automotive front sub-frame," *Journal of Mechanical Engineering*, vol. 52, no. 22, pp. 112–120, 2016.

[3] G. Rongrong, Y. Xue, and X. Niu, "Experimental study on lowcycle fatigue behavior of Chinese LYP225," *China Civil Engineering Journal*, vol. 50, no. 1, pp. 12–19, 2017.

[4] S. Chen, H. Wang, B. Xu, and J. Kang, "Law of rolling contact fatigue life of thermal spray coatings: a review," *Journal of Mechanical Engineering*, vol. 50, no. 8, pp. 23–33, 2014.

[5] J. X. Mao, H. Wang, D. M. Feng, T.-Y. Tao, and W.-Z. Zheng, "Investigation of dynamic properties of long-span cable-stayed bridges based on one-year monitoring data under normal operating condition," *Structural Control and Health Monitoring*, vol. 25, no. 5, p. 2146, 2018.

[6] K. Gouda, P. Rycerz, A. Kadiric, and G. E. Morales-Espejel, "Assessing the effectiveness of data-driven time-domain condition indicators in predicting the progression of surface distress under rolling contact," *Proceedings of the Institution of Mechanical Engineers Part J: Journal of Engineering Tribology*, vol. 233, no. 10, pp. 1523–1540, 2019.

[7] Z. Hua, H. Zhang, Q. Wei, Y. Fan, and S. Pan, "Development a novel fatigue testing apparatus for artificial hip joint femur stem," *Journal of Mechanical Engineering*, vol. 52, no. 1, pp. 160–164, 2016.

[8] W. Tan, R. Xu, L. Mi, and S. Chen, "Design of fatigue life test system of the energy efficient heavy transmission," *Mechanical Drive*, vol. 51, pp. 1–5, 2017.

[9] J. Bai and R. Jian, "Novel method of electro-hydraulic resonant fatigue testing," *Journal of Mechanical Engineering*, vol. 51, no. 2, pp. 161–168, 2015.

[10] X. Li, S. Zhang, C. Pang et al., "Research on testing of materials rolling contact fatigue," *Aviation Precision Manufacturing Technology*, vol. 47, no. 3, pp. 5–7, 2011.

[11] S. Schneider, R. Herrmann, and S. Marx, "Development of a resonant fatigue testing facility for large-scale beams in bending," *International Journal of Fatigue*, vol. 113, pp. 171–183, 2018.

[12] V. Manoj, K. Manohar Shenoy, and K. Gopinath, "Developmental studies on rolling contact fatigue test rig," *Wear*, vol. 264, no. 7-8, pp. 708–718, 2008.

[13] Y. Yang, X. Qi, R. Zhang et al., "Design and development of a rolling contact fatigue test machine for superhard coatings," *Lubrication Engineer*, vol. 3, pp. 5–7, 2011.

[14] L. Wang, S. Cheng, C. Pang et al., "Development of BFT-10000 fatigue tester," *Aviation Precision Manufacturing Technology*, vol. 50, no. 3, pp. 42–46, 2014.

[15] H. You, "Control system design of hydraulic fatigue testing machine based on double lower computers," *Control Engineering of China*, vol. 21, no. 2, pp. 215–218, 2014.

[16] L. Tao, Y. Gu, B. Xu et al., "Development of automation-control system to test fatigue performance of metallic material," *Instrument Technique and Sensor*, vol. 5, pp. 54–72, 2016.

[17] S. Lu, L. Hui, M. Fan et al., "Electricloading system with multi closed-loop control," *Electric Machines and Control*, vol. 19, no. 9, pp. 16–22, 2015.

[18] I. Bodini, G. Sansoni, M. Lancini, S Pasinetti, and F Docchio, "Feasibility study of a vision system for on-line monitoring of rolling contact fatigue tests," *Journal of Physics: Conference Series*, vol. 778, no. 1, Article ID 012007, 2017.

[19] X. Liu and L. Zhao, "Method to restrain extra torque of aircraft rudder electric loading system," *Systems Engineering Electronics*, vol. 41, no. 6, pp. 1366–1373, 2019.

[20] X. Hou, G. Zhang, J. Wang et al., "Driving control system design of continuous flat press based on SIMOTION D435," *Scientia Silvae Sinicae*, vol. 54, no. 4, pp. 116–126, 2018.

[21] X. Sun, H. Tan, A. Yang et al., "Multi-axis synchronous motion control system based on SIMOTION for industrial computed tomography," *Control Engineering of China*, vol. 23, no. 10, pp. 1591–1596, 2016.

[22] W. Wang, Q. Lu, and X. Zhang, *Explanation for SIEMENS Motion Controller: SIMOTION Hangbook*, Machine Press, Beijing, China, 2nd edition, 2013.